chemosensors

MDPI

Article

Preparation and Photoluminescent Properties of Tb^{3+}-Doped $Lu_2W_3O_{12}$ and $Lu_2Mo_3O_{12}$ Green Phosphors

Nihui Huang [1], Guojun Lu [2], Bihai Bai [1], Zijun Chen [1], Min Zhang [1], Yuechan Li [1], Chunyan Cao [1,*] and An Xie [1]

[1] Fujian Key Laboratory of Functional Materials and Applications, School of Materials Science and Engineering, Xiamen University of Technology, Xiamen 361024, China
[2] Department of Fundamental Courses, Xiamen Donghai Institute, Xiamen 361112, China
* Correspondence: caoyan_80@t.xmut.edu.cn

Abstract: Tungstate and molybdate phosphors have received great attention for their excellent photoluminescent properties and thermal stabilities. In the article, Tb^{3+}-activated tungstate and molybdate green phosphors were prepared by a solid-state reaction method at different caline temperatures and were compared and studied. The crystal structures and the morphologies of samples were characterized by X-ray diffraction (XRD) patterns and field emission scanning electron microscopy (FE-SEM) images. The energy-dispersive spectra (EDS) proved the compositions of the prepared samples. The photoluminescence (PL) spectra showed that the PL excitation spectra of Tb^{3+}-doped $Lu_2W_3O_{12}$ and $Lu_2Mo_3O_{12}$ green phosphors consisted of a broad and strong charge transfer band (CTB) and 4f–5d transitions of Tb^{3+} in the ultraviolet (UV) wavelength range and some narrowed excitation peaks from the 4f–4f transition of Tb^{3+} in the near ultraviolet (NUV) wavelength region. The PL emission spectra of the phosphors exhibited the characteristic green emissions owing to the $^5D_4 \rightarrow {}^7F_5$ transition of Tb^{3+} located at about 547 nm. The values of energy gap E_g were calculated based on the diffuse reflection spectra (DRS). The measuring temperature-dependent PL spectra illustrated the thermal stabilities of phosphors. The Tb^{3+}-doped $Lu_2Mo_3O_{12}$ phosphor presented normal thermal quenching phenomena and the values of the thermal activation energy E_a were calculated based on the measuring temperature dependent PL emission spectra. The Tb^{3+}-doped $Lu_2W_3O_{12}$ phosphor exhibited abnormal thermal enhancing CTB excitation intensity at about 170 °C. Furthermore, the PL decay curves suggested that the lifetime corresponding to the $^5D_4$ level of Tb^{3+} in the $Lu_2W_3O_{12}$ host lattice was longer than that in the $Lu_2Mo_3O_{12}$ host lattice. Compared the Tb^{3+}-doped $Lu_2Mo_3O_{12}$ phosphor, the Tb^{3+}-doped $Lu_2W_3O_{12}$ phosphor has shown potential as an application in temperature sensors.

Keywords: tungstate phosphors; molybdate phosphors; luminescent properties; thermal stabilities; Tb^{3+}

check for updates

Citation: Huang, N.; Lu, G.; Bai, B.; Chen, Z.; Zhang, M.; Li, Y.; Cao, C.; Xie, A. Preparation and Photoluminescent Properties of Tb^{3+}-Doped $Lu_2W_3O_{12}$ and $Lu_2Mo_3O_{12}$ Green Phosphors. *Chemosensors* **2022**, *10*, 533. https://doi.org/10.3390/chemosensors10120533

Academic Editor: Marco Frasconi

Received: 21 October 2022
Accepted: 12 December 2022
Published: 14 December 2022

Publisher's Note: MDPI stays neutral with regard to jurisdictional claims in published maps and institutional affiliations.

Copyright: © 2022 by the authors. Licensee MDPI, Basel, Switzerland. This article is an open access article distributed under the terms and conditions of the Creative Commons Attribution (CC BY) license (https://creativecommons.org/licenses/by/4.0/).

1. Introduction

In recent years, "double carbon" has once again become a hot topic, and many have made contributions to energy conservation and carbon reduction, saving electric energy more effectively and helping to achieve the goal of "double carbon". As far as illumination is concerned, the key lies in the correct selection of high-efficiency phosphors that can emit good visible light. This requires the luminous efficiency and working stability of fluorescent phosphors. Phosphors have strong practical and scientific interest for scientists. Much of the literature concerning rare earth phosphors has reported on its wide applications [1–4]. Phosphors are classified by matrixes such as oxides, nitrides, phosphates, fluorides, borates, sulfates, aluminates, silicates, sulfides, tungstates, vanadates, molybdates, etc. Host materials with the values of energy band gaps E_g between 3 eV and 5 eV are considered to be the best host matrix for phosphors [5]. Among these phosphors, tungstate phosphors and the molybdate phosphors are considered to be promising phosphors, owing to their high physical and chemical stability as well as thermal stabilities [6,7]. In addition, the WO_4^{2-},

WO_6^{6-}, MoO_4^{2-}, and MoO_6^{6-} groups can efficiently absorb ultraviolet (UV) light through the excitation of the $O^{2-}-W^{6+}$ and $O^{2-}-Mo^{6+}$ charge transfer absorption [8–11]. The excitation energy can be transferred to luminescent ions, such as Eu^{3+} and Sm^{3+}, and then emit red light. There are some reports on rare earth molybdate phosphors and tungstate phosphors [12–14].

Few reports on Tb^{3+}-doped molybdate phosphors or tungstate phosphors were reported [15,16]. The Tb^{3+}-doped materials are usually used as green phosphors because of their bright $^5D_4 \rightarrow {}^7F_5$ emissions, which peak at about 544 nm in the green spectral region. To the best of our knowledge, the investigations on the Tb^{3+}-doped $Lu_2W_3O_{12}$ and $Lu_2Mo_3O_{12}$ phosphors have been rarely reported. For phosphors, thermal quenching is a normal phenomenon for nonradiative transitions at higher temperatures, which is also a drawback for practical applications such as display, lighting, and photovoltaics [17]. Recently, thermally stable phosphors that conquered or were weak were reported as drawbacks [18,19]. Further, thermal enhancement up-conversion emissions in $Yb_2W_3O_{12}$ and $Sc_2Mo_3O_{12}$ materials were reported and the enhancement was attributed to the negative thermal expansion (NTE) [20,21]. When the up-conversion materials are integrated into biological sensors or optoelectronic devices, the thermally enhanced up-conversion luminescence can provide enhanced detection sensitivities and improved energy conversion efficiencies. Enhanced Eu^{3+} emissions were also reported in $Lu_2(MoO_4)_3$ phosphors [22,23]. Above 450 K, the $Lu_2(MoO_4)_3$ shows a very intense NTE phenomenon [24]. What about the Tb^{3+} emission in $Lu_2W_3O_{12}$ and $Lu_2Mo_3O_{12}$ host matrices?

In this work, the Tb^{3+}-doped and undoped $Lu_2W_3O_{12}$ and $Lu_2Mo_3O_{12}$ green phosphors were prepared through a solid-state reaction method. The crystalline structures, the morphologies, the compositions, the diffuse reflectance spectra, the room temperature and high temperature photoluminescence spectra, the thermal stabilities, and the luminescent decay curves of Tb^{3+}-doped $Lu_2W_3O_{12}$ and $Lu_2Mo_3O_{12}$ green phosphors were compared and studied.

2. Experimental Section

2.1. Materials

Lu_2O_3 (99.99%, Aladdin), Tb_4O_7 (99.99%, Aladdin), WO_3 (99.99%, Aladdin), and MoO_3 (99.9%, Aladdin) were used as raw materials without further purification to prepare the Tb^{3+}-doped and undoped $Lu_2W_3O_{12}$ and $Lu_2Mo_3O_{12}$ materials.

2.2. Preparation and Characterization

The Tb^{3+}-doped and undoped $Lu_2W_3O_{12}$ and $Lu_2Mo_3O_{12}$ materials were prepared through a solid-state reaction method as reported [22,23]. In a typical procedure, for the preparation of 10 mmol of 5 mol% Tb^{3+}-doped $Lu_2W_3O_{12}$, 9.5 mmol of Lu_2O_3, 0.25 mmol of Tb_4O_7, and 30 mmol of WO_3 were weighed and ground thoroughly, placed into a corundum crucible, and calcined at 1000 °C for 4 h in a muffle furnace with some carbon powder in the muffle furnace. When the muffle furnace cooled down to room temperature, the obtained white powder was collected and the phosphor was obtained. For comparison, the 5 mol% Tb^{3+}-doped $Lu_2Mo_3O_{12}$ and undoped $Lu_2W_3O_{12}$ and $Lu_2Mo_3O_{12}$ samples were prepared with the similar procedure except for the raw materials. Calcining temperatures of 800, 900, 1000, 1100, 1200, and 1300 °C were applied to prepare the materials. Under 254 nm or 365 nm UV light, the Tb^{3+}-doped materials emit a bright green light seen by the naked eye, suggesting green phosphors were prepared.

To determine the crystal structure, the X-ray diffraction (XRD) patterns of the prepared phosphors were characterized with CuKα (λ = 1.5406 Å) radiation at 40 kV and 40 mA using a Rigaku Smart lab X-ray diffractometer. The 2θ ranges of the data were all set from 10° to 70° with a step size of 0.02°. A Zeiss field emission scanning electron microscope (FE-SEM) was used to study the morphologies and the particle size. The compositions of the materials were characterized by energy-dispersive spectra (EDS) with the attachment EDS equipment in the FE-SEM. The diffuse reflection spectra (DRS) were obtained on a

visible-near infrared (Vis-NIR) spectrophotometer (UV-2700) with $BaSO_4$ as the standard reference. A Scientific Lumina fluorescence spectrophotometer with a power of 150 W Xe lamp as an excitation source was used to record the photoluminescence (PL) excitation and emission spectra at room temperature. The high temperature dependent PL spectra of obtained phosphors were recorded by the same fluorescence spectrophotometer with a heating equipment TAP-02 (Tian Jin Oriente KOJI Instrument Co., Ltd., Tianjin, China) high-temperature fluorescence attachment. The luminescent decay curves were recorded by a Horiba Scientific FluroMax-4 spectrophotometer with a pulsed 150 W xenon lamp as an excitation source.

3. Results

3.1. Characterization of XRD and Crystal Structure

Figure 1 shows XRD patterns of Tb^{3+}-doped $Lu_2W_3O_{12}$ phosphors prepared at 800, 900, 1000, 1100, 1200, 1300 °C, and reference data. The XRD patterns can be indexed to the $Yb_2Mo_3O_{12}$ with JCPDS card No. 33-1451. Because Lu^{3+} is isostructural to the Yb^{3+} and the W^{6+} has similar electronic structure to that of the Mo^{6+}, it can be inferred that the $Lu_2W_3O_{12}$ phosphor was prepared. When the preparation temperature was 800 °C, the XRD pattern of the obtained material could be indexed to the reference data of $Yb_2Mo_3O_{12}$ well. When the preparation temperature increased with 100 °C intervals up to 1300 °C, all the XRD patterns could be indexed to the reference data. The full width at half maximum (FWHM) of the diffraction peak became narrower and the diffraction intensity became stronger with the increase of preparation temperature. The XRD measurement results suggested that the Tb^{3+}-doped $Lu_2W_3O_{12}$ phosphors can be prepared from 800 °C to 1300 °C.

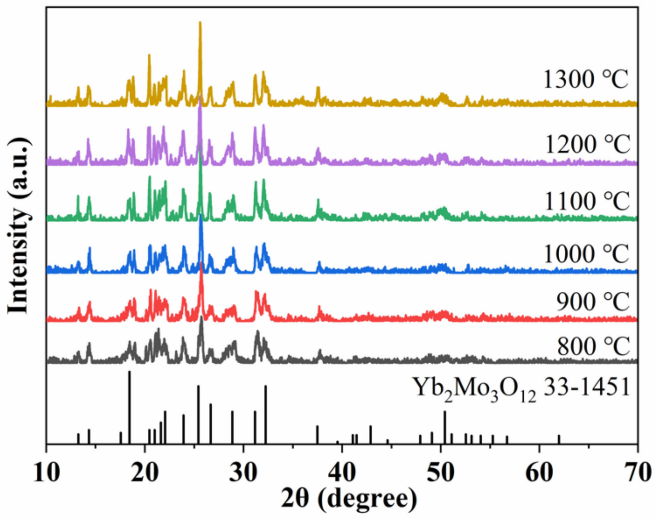

Figure 1. Preparation of temperature-dependent XRD patterns of Tb^{3+}-doped $Lu_2W_3O_{12}$ and reference data.

The preparation of temperature-dependent XRD patterns of Tb^{3+}-doped $Lu_2Mo_3O_{12}$ phosphors and the reference data are shown in Figure 2. Based on the analysis of [23] and the measurement results, the XRD patterns of Tb^{3+}-doped $Lu_2Mo_3O_{12}$ phosphors prepared at different preparation temperatures can all be well indexed to the reference data of $Yb_2Mo_3O_{12}$ with JCPDS card No. 33-1451. Similar to those of the Tb^{3+}-doped $Lu_2W_3O_{12}$ phosphors, with the increase of preparation temperature, the full width at half maximum of the XRD diffraction peak became narrower and the diffraction intensity gradually increased. The results show that the Tb^{3+}-doped $Lu_2Mo_3O_{12}$ phosphors were obtained when the preparation temperature varied from 800 °C to 1300 °C.

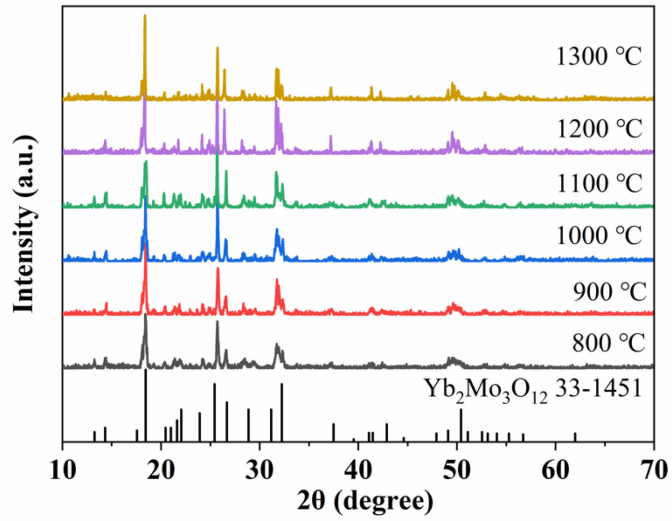

Figure 2. Preparation of temperature-dependent XRD patterns of Tb^{3+}-doped $Lu_2Mo_3O_{12}$ and reference data.

Figure 3 shows the XRD patterns of 5 mol% Tb^{3+}-doped and undoped $Lu_2W_3O_{12}$ and $Lu_2Mo_3O_{12}$ powders prepared at 1000 °C and the reference data. Referring to the preparation of the temperature-dependent XRD patterns of Tb^{3+}-doped $Lu_2W_3O_{12}$ and $Lu_2Mo_3O_{12}$ phosphors, the XRD patterns of the 5 mol% Tb^{3+}-doped and undoped $Lu_2W_3O_{12}$ and $Lu_2Mo_3O_{12}$ samples can be well indexed to $Yb_2Mo_3O_{12}$ with JCPDS card No. 33-1451. Comparing the Tb^{3+}-doped and undoped XRD patterns of the $Lu_2W_3O_{12}$ and $Lu_2Mo_3O_{12}$ powders, the Tb^{3+} doping did not cause apparent variations on the patterns, with the exception of the diffraction intensities.

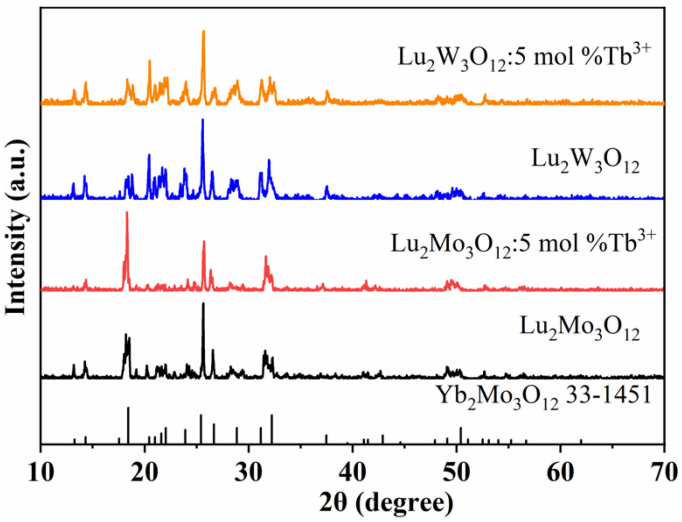

Figure 3. XRD patterns of 5 mol%Tb^{3+}-doped and undoped $Lu_2W_3O_{12}$ and $Lu_2Mo_3O_{12}$ materials prepared at 1000 °C and reference data.

Figure 4a,b display schematic crystal structure diagrams of $Lu_2W_3O_{12}$ and $Lu_2Mo_3O_{12}$, respectively. As is illustrated, Lu^{3+} is bonded to six O^{2-} to form LuO_6 octahedra and W^{6+} or Mo^{6+} is bonded to four O^{2-} to form WO_4^{2-} or MoO_4^{2-} tetrahedra. The $Lu_2W_3O_{12}$ or $Lu_2Mo_3O_{12}$ crystal is composed of corner-sharing LuO_6^{6-} octahedra and WO_4^{2-} or MoO_4^{2-} tetrahedra. One LuO_6 octahedra shares corners with six WO_4 tetrahedra. With the temperature increasing, the Lu-O-W and Lu-O-Mo will rotate, resulting in the shrinkage of the $Lu_2W_3O_{12}$ and $Lu_2Mo_3O_{12}$ crystal lattice, which present the NTE phenomena. After doping 5 mol% Tb^{3+}, the Tb^{3+} ions replace the Lu^{3+} ions in the $Lu_2W_3O_{12}$ and $Lu_2Mo_3O_{12}$

crystals for the similarity of Tb^{3+} to Lu^{3+}. The contraction of the crystal lattice will affect the emissions of Tb^{3+} at high temperatures.

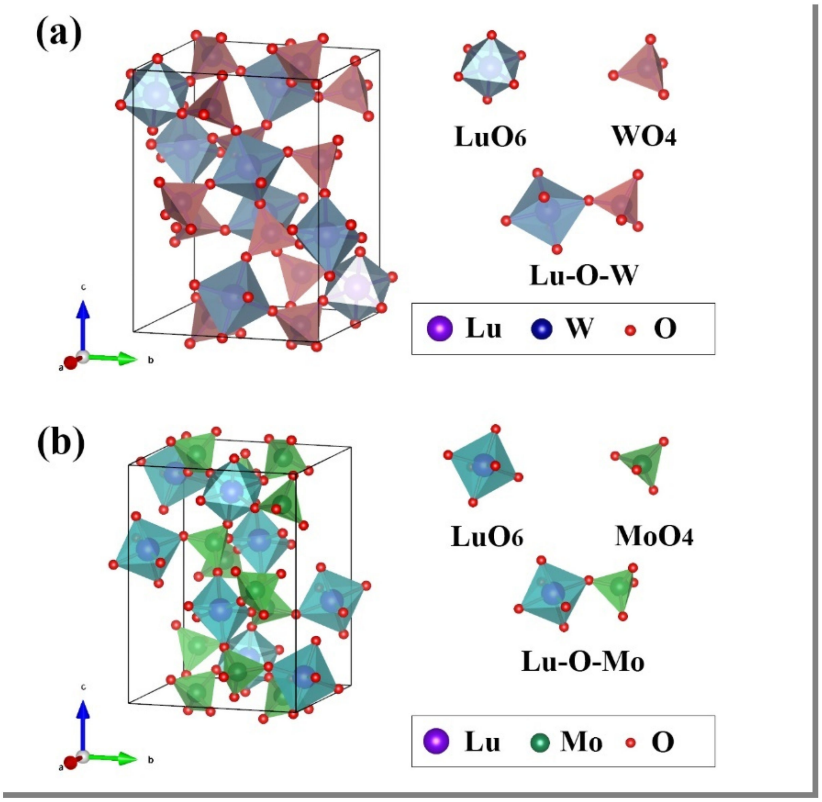

Figure 4. Schematic crystal structure diagrams of $Lu_2W_3O_{12}$ (**a**) and $Lu_2Mo_3O_{12}$ (**b**).

3.2. Composition and Morphology Characterization

Figure 5 presents the FE-SEM images and EDS spectra of an undoped $Lu_2Mo_3O_{12}$ sample (a,b), a 5 mol% Tb^{3+}-doped $Lu_2Mo_3O_{12}$ phosphor (c,d), undoped $Lu_2W_3O_{12}$ material (e,f), and a 5 mol% Tb^{3+}-doped $Lu_2W_3O_{12}$ phosphor (g,h) prepared at 1000 °C, respectively. For convenient comparison, the scales bars were all 2 μm in the FE-SEM images, and all the FE-SEM images were captured under the same magnifications. The undoped $Lu_2Mo_3O_{12}$ micron particles in Figure 5a were well dispersed with good homogeneity, non-agglomeration, uniformity in size distribution, and with a sphere-like morphology. Through a Nano Measurer software dealing, the average size of the particles was about 2.14 μm. The corresponding EDS spectrum in Figure 5b indicates that the material contains Lu, Mo, and O. After some Tb^{3+} was introduced into $Lu_2Mo_3O_{12}$ lattice, the morphology of the micro-particles (Figure 5c) did not change much and the average size of the particles was about 2.17 μm. Tb^{3+} was detected in the corresponding EDS pattern (Figure 5d). The $Lu_2W_3O_{12}$ was composed of some undefined and unsmoothed particles and some irregular agglomeration nanoparticles appeared on the surface of the particles (Figure 5e). Compared with $Lu_2Mo_3O_{12}$ material, the $Lu_2W_3O_{12}$ sample possessed smaller particles and the average size of the particles was about 1.42 μm. The corresponding EDS pattern in Figure 5f indicates that the material contains Lu, W, and O. After 5 mol%, Tb^{3+} was introduced in $Lu_2W_3O_{12}$ (Figure 5g), and the morphology of the sample did not change significantly, and the average size of the particles was about 1.19 μm. The Tb element was also detected in addition to Lu, W, and O in the corresponding EDS pattern, as shown in Figure 5h. The FE-SEM images suggest that the $Lu_2Mo_3O_{12}$ samples have bigger size particles than those $Lu_2W_3O_{12}$ samples. Tb^{3+} doping did not lead to apparent changes in the particle morphologies nor in their the sizes. The EDS patterns proved the compositions of the samples. The Tb^{3+} doping did affect the PL properties greatly.

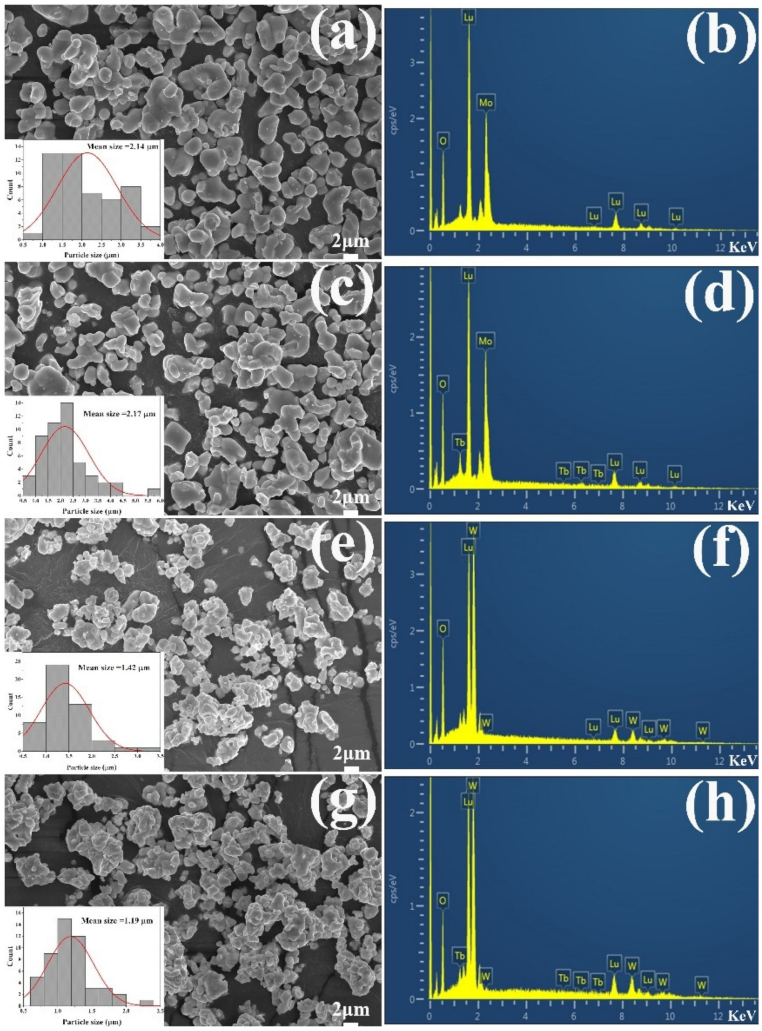

Figure 5. FE-SEM images and EDS spectra of undoped $Lu_2Mo_3O_{12}$ (**a**,**b**), 5 mol% Tb^{3+}-doped $Lu_2Mo_3O_{12}$ (**c**,**d**), undoped $Lu_2W_3O_{12}$ (**e**,**f**), and 5 mol% Tb^{3+}-doped $Lu_2W_3O_{12}$ (**g**,**h**) prepared at 1000 °C. Insets in FE-SEM images are corresponding particle size distribution statistics.

3.3. PL Properties

The preparation of temperature-dependent PL excitation spectra of Tb^{3+}-doped $Lu_2W_3O_{12}$ monitored at $^5D_4 \rightarrow {}^7F_5$ emission are shown in Figure 6. With the preparation temperature increased from 800 °C to 1300 °C, all PL excitation spectra show broad excitation bands in the wavelength range of 200 nm to 330 nm, which can be attributed to the O^{2-}-W^{6+} charge transfer band (CTB) transition from host $[WO_4]^{2-}$ and the 4f–5d transition of Tb^{3+} [25,26]. The excitation intensities of CTB and 4f–5d transition of Tb^{3+} increased firstly, and reached the maxima at 1200 °C, and then decreased when the temperature increased to 1300 °C. The narrow weak excitation peaks in the wavelength range of 330 nm to 500 nm originated from the 4f–4f transition absorption of Tb^{3+}. Comparing the samples prepared at 900 °C and higher temperatures, the 4f–4f transition absorptions of Tb^{3+} prepared at 800 °C were very weak, suggesting that the Tb^{3+} was not successfully doped into the host lattice. The phosphor prepared at 900 °C presented apparent Tb^{3+} 4f–4f transition absorptions. In addition, the intensities of CTB and 4f–5d of Tb^{3+} transitions were much stronger than those of the 4f–4f transition of Tb^{3+}. The PL excitation spectra suggests that the optimum preparation temperature is 1200 °C for Tb^{3+}-doped $Lu_2W_3O_{12}$ phosphors.

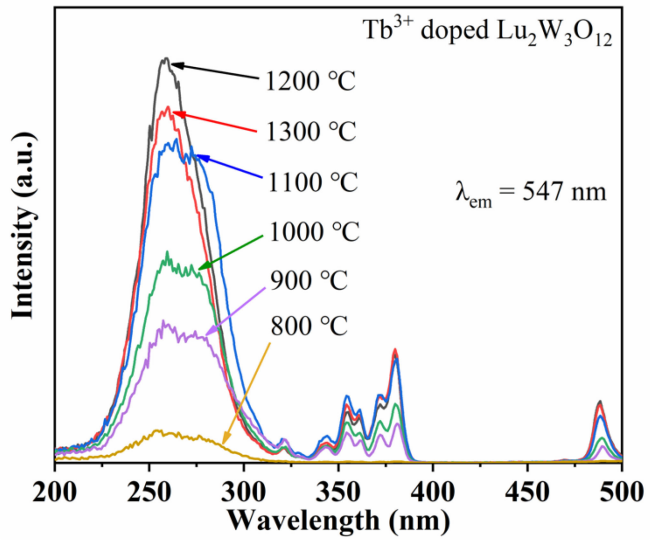

Figure 6. Preparation of temperature-dependent PL excitation spectra of Tb^{3+}-doped $Lu_2W_3O_{12}$ phosphors.

Figure 7 shows the preparation of the temperature-dependent PL excitation spectra of Tb^{3+}-doped $Lu_2Mo_3O_{12}$. By monitoring the $^5D_4 \rightarrow {}^7F_5$ emission at 547 nm, the PL excitation spectra of phosphor prepared at different preparation temperature shows a strong and broad excitation band in the wavelength range from 200 nm to 330 nm, which can be attributed to O^{2-}-Mo^{6+} CTB transition from host $[MoO_4]^{2-}$ at about 260 nm and the 4f–5d transition of Tb^{3+} located at about 282 nm. With the preparation temperature increasing, the relative CTB excitation intensities of the O^{2-}-Mo^{6+} and 4f–5d transition of Tb^{3+} changed. The O^{2-}-Mo^{6+} CTB was superior in the phosphors prepared at 800, 900, and 1000 °C, whereas for the phosphors prepared at 1100, 1200, and 1300 °C, the 4f–5d transition of Tb^{3+} prevailed. In addition, with the preparation temperature increased from 800 °C to 1300 °C, the excitation intensity of CTB increased firstly and then decreased, reaching the maxima at 1100 °C. For the excitation peaks originating from the 4f–4f transitions of Tb^{3+} located in the wavelength range of 330 nm to 500 nm, the intensities of the excitations increased with the calcine temperature increasing. Unlike the PL excitation intensities of Tb^{3+}-doped $Lu_2W_3O_{12}$, the intensities of CTB and the 4f–5d transitions of Tb^{3+} were similar to those of the 4f–4f transitions of Tb^{3+}.

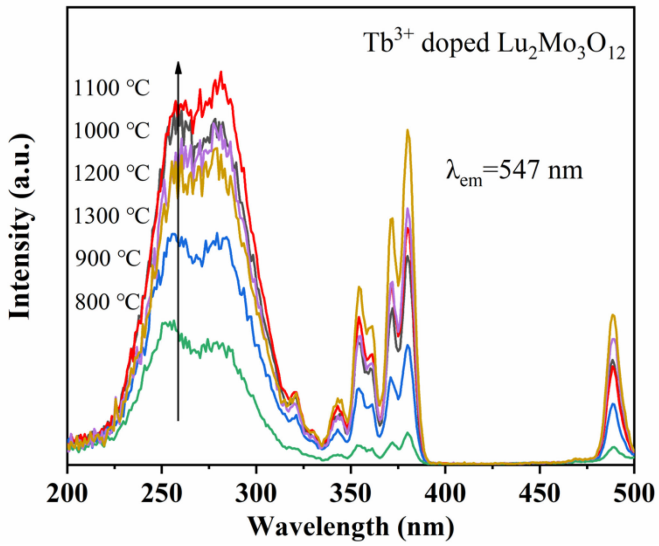

Figure 7. Preparation of temperature-dependent PL excitation spectra of Tb^{3+}-doped $Lu_2Mo_3O_{12}$ phosphors.

As is shown in Figure 7, the CTB excitation intensity of the Tb^{3+}-doped $Lu_2Mo_3O_{12}$ phosphors prepared at 1000 °C and 1100 °C were similar. Considering the principle of energy saving and the safety in lab, 1000 °C was selected as the preparation temperature to prepare and compare the Tb^{3+}-doped $Lu_2Mo_3O_{12}$ and $Lu_2W_3O_{12}$ phosphors.

Figure 8 shows the PL excitation and emission spectra of 5 mol% Tb^{3+}-doped $Lu_2W_3O_{12}$ and $Lu_2Mo_3O_{12}$ phosphors. By monitoring the 547 nm emission corresponding to the $^5D_4 \rightarrow {}^7F_5$ transition of Tb^{3+}, the PL excitation spectra are composed of two parts. One part is a strong and broad excitation band in the wavelength range of 200–330 nm. There is one peak located at about 260 nm, which is generated by the O^{2-} (2p)–W^{6+} (5d) or O^{2-} (2p)–Mo^{6+} (4d) CTB transition from host $[WO_4]^{2-}$ or $[MoO_4]^{2-}$ groups. In addition, there is a peak at about 275 nm (or 282 nm), which originates from the Tb^{3+} 4f–5d transition [25,26]. The existence of the CTBs and the spectral overlap of the excitation spectra suggest the energy transfer between the $[WO_4]^{2-}$ or $[MoO_4]^{2-}$ groups and Tb^{3+}. In the wavelength of 330 nm to 500 nm, there are characteristic 4f–4f transitions of Tb^{3+} peaked at 321, 344, 354, 361, 372, and 380 nm, corresponding to the transitions of the $^7F_6 \rightarrow {}^5D_0$, $^7F_6 \rightarrow {}^5G_2$, $^7F_6 \rightarrow {}^5D_2$, $^7F_6 \rightarrow {}^5G_5$, $^7F_6 \rightarrow {}^5G_6$, and $^7F_6 \rightarrow {}^5D_3$ transitions [27], respectively. The strongest one peaked at 380 nm in the near-ultraviolet (NUV) region, which suggests that the $Lu_2W_3O_{12}$ and $Lu_2Mo_3O_{12}$ phosphors can be excited by NUV LED chips. For the Tb^{3+}-doped $Lu_2W_3O_{12}$ and $Lu_2Mo_3O_{12}$ phosphors, with 260 nm and 380 nm excitation, four emission peaks at 492, 547, 586, and 622 nm originating from the $^5D_4 \rightarrow {}^7F_6$, $^5D_4 \rightarrow {}^7F_5$, $^5D_4 \rightarrow {}^7F_4$, $^5D_4 \rightarrow {}^7F_3$ transitions of Tb^{3+} are recorded. The $^5D_4 \rightarrow {}^7F_5$ transition that peaked at 547 nm is the strongest emission, and the phosphors yielded a bright green light. The insets are the corresponding photographs captured under the illumination of 254 nm light in a camera obscura, which indicate the successful preparation of green phosphors.

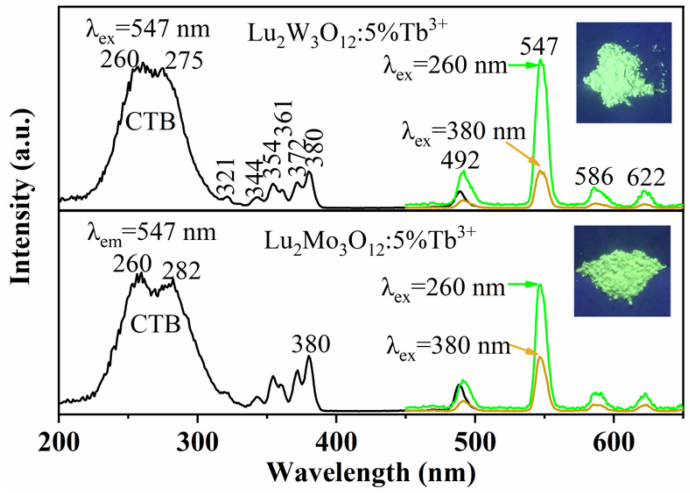

Figure 8. PL excitation and emission spectra of 5 mol%Tb^{3+}-doped $Lu_2W_3O_{12}$ and $Lu_2Mo_3O_{12}$ phosphors prepared at 1000 °C. Inserts are the corresponding phosphor pictures captured under 254 nm light.

Under 254 nm light, the $Lu_2W_3O_{12}$ phosphor produced a stronger bright green light than that of the $Lu_2Mo_3O_{12}$ phosphor seen by the naked eye. To confirm that, Figure 9 displays the PL excitation spectra of the two phosphors which were recorded under the same measurement conditions. By monitoring at 547 nm emission of the transition $^5D_4 \rightarrow {}^7F_5$ of Tb^{3+}, the $Lu_2W_3O_{12}$ phosphor presented about 1.5 times the excitation intensity of CTBs and Tb^{3+} 4f–5d transitions than those of the $Lu_2Mo_3O_{12}$ phosphor. Yet, the two phosphors illustrated the similar intensities of Tb^{3+} 4f–4f transitions. When the preparation temperature was 1000 °C, $Lu_2W_3O_{12}$ phosphor was a better choice than $Lu_2Mo_3O_{12}$ phosphor for CTB excitation.

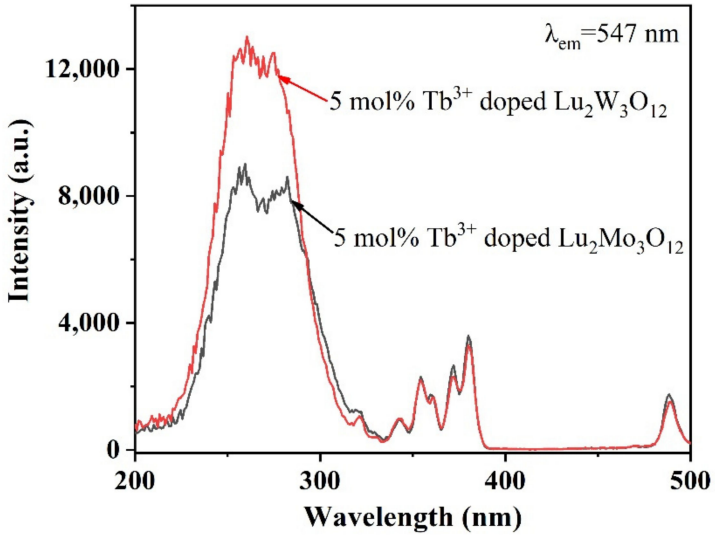

Figure 9. Comparison of PL excitation spectra of 5 mol% Tb^{3+}-doped $Lu_2W_3O_{12}$ and $Lu_2Mo_3O_{12}$ phosphors prepared at 1000 °C.

3.4. DRS

The DRS of 5 mol% Tb^{3+}-doped and undoped $Lu_2W_3O_{12}$ and $Lu_2Mo_3O_{12}$ materials are shown in Figure 10. All the materials have low reflectance in the wavelength range of 200–350 nm, which mean the materials have strong absorptions in the wavelength range. The absorptions can be attributed to the CTBs of O^{2-}-W^{6+} or O^{2-}-Mo^{6+} and Tb^{3+} 4f–5d transitions. As can be seen from Figure 10, the incorporation of Tb^{3+} caused the movements of the absorptions to short wavelength range. The energy gap value E_g of the materials can be estimated from DRS by using equation [28]:

$$(\alpha h\upsilon)^n = c(h\upsilon - E_g) \quad (1)$$

where α, h, υ, and c are the absorption coefficient, the Planck's constant, the incident light frequency and a constant, respectively. The value of n is 2 or 1/2, depending on the transition mode of the material, and n = 2 is a direct transition, whereas n = 1/2 is an indirect transition. The absorption coefficient α can be solved by using the Kubelka–Munk equation [29]:

$$F(R) = \frac{(1-R)^2}{2R} = \frac{K}{S} \quad (2)$$

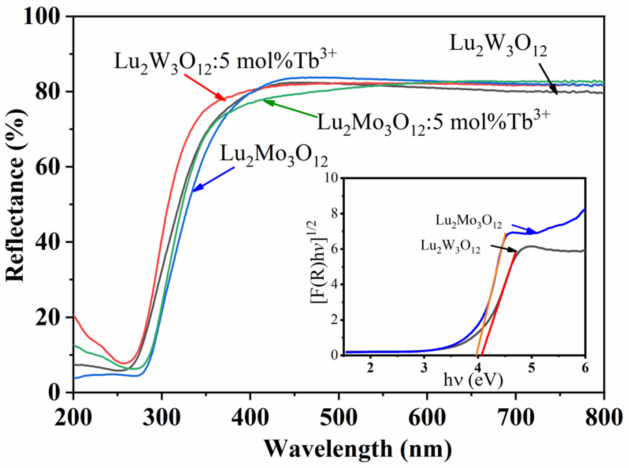

Figure 10. DRS of 5 mol% Tb^{3+}-doped and undoped $Lu_2W_3O_{12}$ and $Lu_2Mo_3O_{12}$ materials. Inserts display $[F(R)h\nu]^{1/2}$-hν plots of undoped $Lu_2W_3O_{12}$ and $Lu_2Mo_3O_{12}$ samples prepared at 1000 °C.

In this function, the reflection coefficient R is recorded by DRS, S is the scattering coefficient and independent on the wavelength of the incident light, and the value of K is proportional to α in Equation (1). In this case, n equals 1/2 and $Lu_2W_3O_{12}$ [30] and $Lu_2Mo_3O_{12}$ [31] are both indirect bandgap materials. By plotting $[F(R)h\nu]^{1/2}$ versus $h\nu$, the value of E_g can be obtained. The insert in Figure 10 presents the $[F(R)h\nu]^{1/2}$-$h\nu$ plots of undoped $Lu_2W_3O_{12}$ and $Lu_2Mo_3O_{12}$ samples. By extrapolating $F(R)$ to 0, the values of E_g of 4.02 eV and 3.94 eV for undoped $Lu_2W_3O_{12}$ and $Lu_2Mo_3O_{12}$ samples were obtained, respectively. For 5 mol% Tb^{3+}-doped $Lu_2W_3O_{12}$ and $Lu_2Mo_3O_{12}$ phosphors, the obtained values of E_g were 4.06 eV and 3.95 eV. The value E_g of the $Lu_2W_3O_{12}$ material was larger than that of the $Lu_2Mo_3O_{12}$ material, and the value E_g of the doped material was larger than that of corresponding undoped material. The wide band gap is good for luminescent materials [32].

3.5. Measuring Temperature Dependent Spectra, Activation Energy, and Decay Curves

Thermal stability is usually used to evaluate phosphors [33,34]. Figure 11 shows the measuring of temperature-dependent PL excitation spectra of Tb^{3+}-doped $Lu_2Mo_3O_{12}$ phosphors by monitoring at a 547 nm emission of Tb^{3+}. With the measuring temperature increasing from 50 °C to 250 °C, all the intensities of the excitation peaks became weaker. Correspondingly, the emission intensity decreased as well. The thermal luminescence quenching is usually caused by non-radiative transitions at high working temperature [35,36]. At a normal working temperature about 150 °C, the $Lu_2Mo_3O_{12}$ phosphor kept 86% and 76% intensity of that at 50 °C with 260 nm and 380 nm excitations, respectively. Put another way, the emission intensity reduces to 50% of the initial intensity defined as quenching temperature $T_{0.5}$ [37]. In the $Lu_2Mo_3O_{12}$ phosphor, the $T_{0.5}$ is 215 °C and 192 °C with 260 nm and 380 nm excitations.

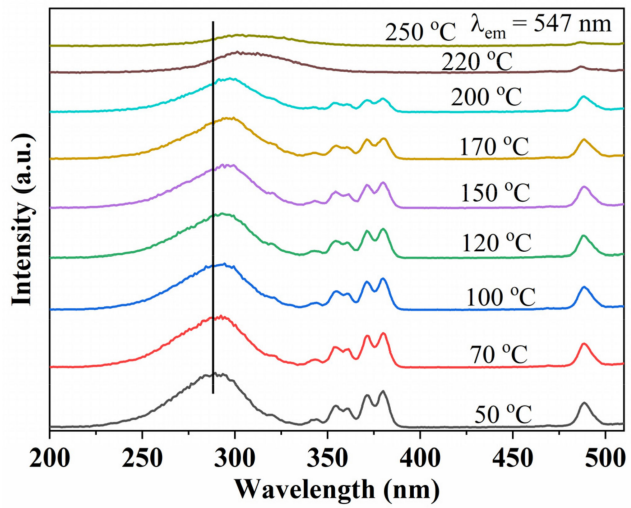

Figure 11. Measuring of temperature-dependent PL excitation spectra of Tb^{3+}-doped $Lu_2Mo_3O_{12}$ phosphor prepared at 1000 °C.

The activation energy (E_a) of the $Lu_2Mo_3O_{12}$ phosphor was also evaluated by using the Arrhenius formula [38]:

$$I_T = \frac{I_0}{1 + c\exp(-E_a/kT)} \quad (3)$$

where I_0 is the initial emission intensity of Tb^{3+}, I_T is the emission intensity of Tb^{3+} at temperature T, c is the quenching frequency factor, and k is the Boltzmann constant and equals 8.617×10^{-5} eV/K [39]. Evolving the formular to $\ln[(I_0/I_T) - 1] = (-E_a/k)(1/T) + c_1$, plotting $\ln[(I_0/I_T) - 1]$ corresponding 1/T, and linear fitting, the $-E_a/k$ can be determined. Further, the E_a value can be obtained. As shown in Figure 12, the data obtained at high temperatures of 220 °C and 250 °C decayed rapidly and the data were not used in the

fitting procedure. The values of $-E_a/k$ were −2340 and −4656 with 260 nm and 380 nm excitations, respectively. Correspondingly, the values of E_a were 0.202 eV and 0.401 eV with 260 nm and 380 nm excitations. The results suggest that the Tb^{3+}-doped $Lu_2Mo_3O_{12}$ phosphor has wonderful thermal stabilities.

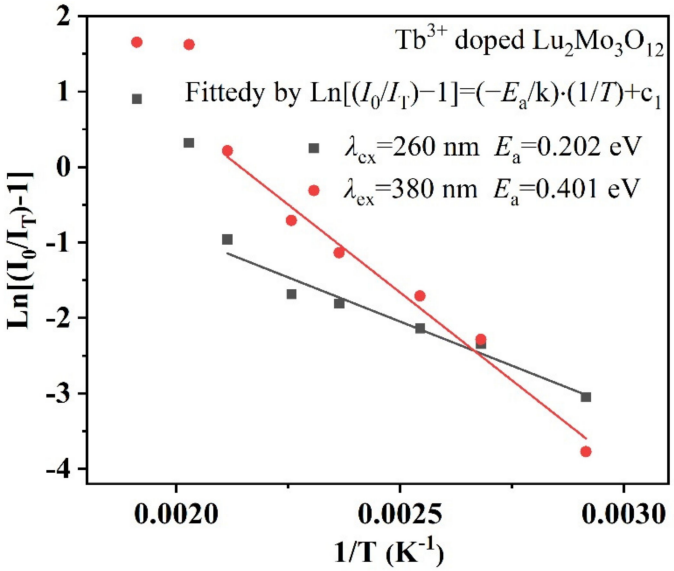

Figure 12. Plots of ln[(I_0/I_T)1] corresponding to 1/T in Tb^{3+}-doped $Lu_2Mo_3O_{12}$ phosphor prepared at 1000 °C.

Unlike the Tb^{3+}-doped $Lu_2Mo_3O_{12}$, the Tb^{3+}-doped $Lu_2W_3O_{12}$ presents a different thermal behavior. For clarity, the measuring temperature and the monitoring wavelength were placed in the temperature-axis with the front number representing the measuring temperature and the latter number representing the monitoring wavelength. As shown in Figure 13, with the measuring temperature increasing, the PL excitation intensity varied differently by monitoring at the $^5D_4 \rightarrow {}^7F_5$ transition. The intensities of Tb^{3+} 4f–4f transitions always decreased with the temperature increasing from 50 °C to 300 °C. Yet, the intensity of the CTB transition decreased with the temperature increasing to 150 °C. When the temperature increased further, the CTB and the Tb^{3+} 4f–5d transitions increased suddenly at about 170 °C and were hardly unchanged, even when the temperature was increased to 300 °C. Furthermore, the peak wavelength of the $^5D_4 \rightarrow {}^7F_5$ transition varied from 546 nm to 552 nm with the measuring temperature increasing. Similar phenomena have been reported in Eu^{3+}-doped $Lu_2(MoO_4)_3$ [22,23]. The enhancing luminescence of Eu^{3+} in $Lu_2(MoO_4)_3$ was recorded at about 250 °C, yet the enhancing luminescence of Tb^{3+} in $Lu_2W_3O_{12}$ was recorded at about 170 °C. The enhancing temperature was lowered to about 80 °C, which was closer to practical applications. The enhancing luminescence has a relationship with the NTE property of the $Lu_2W_3O_{12}$ crystal lattice.

The fluorescent decay curves of the Tb^{3+}-doped $Lu_2W_3O_{12}$ and $Lu_2Mo_3O_{12}$ phosphors by monitoring at 547 nm with 260 nm excitation are shown in Figure 14. The two decay curves can both be fitted by a single exponential function:

$$I(t) = I_0 \exp(-t/\tau) + c \quad (4)$$

where I_0, $I(t)$, τ, and c are emission intensity at initial time, emission intensity at t time, the corresponding fluorescent lifetime, and the background or zero offset, respectively. The fitted lifetimes were 0.724 ms and 0.689 ms for the 5 mol% Tb^{3+}-doped $Lu_2W_3O_{12}$ and $Lu_2Mo_3O_{12}$ phosphors, respectively. The results suggest that the lifetime corresponding to the $^5D_4$ level of Tb^{3+} was longer in the $Lu_2W_3O_{12}$ host lattice than in the $Lu_2Mo_3O_{12}$ host lattice, which is similar to those reported.

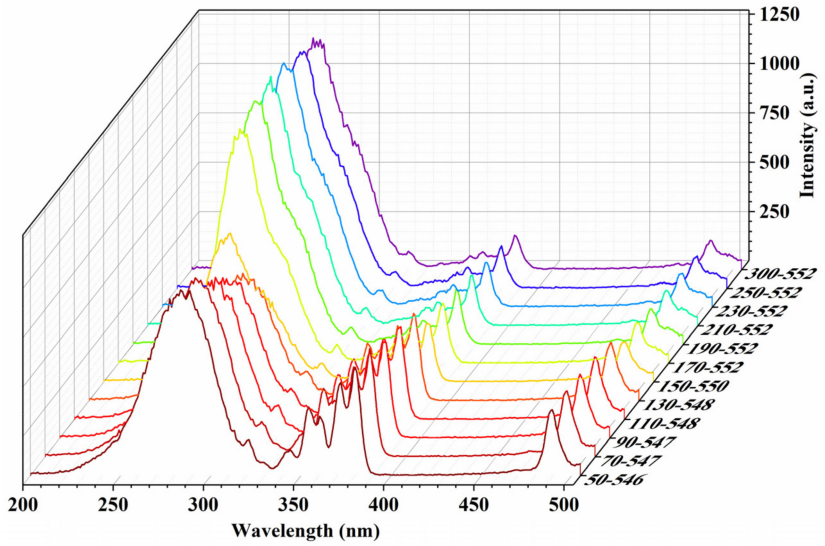

Figure 13. Measuring temperature-dependent PL excitation spectra of Tb^{3+}-doped $Lu_2W_3O_{12}$ prepared at 1000 °C.

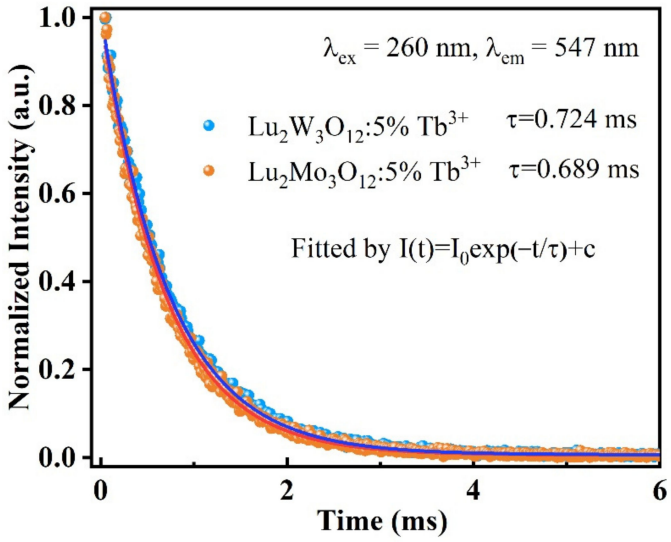

Figure 14. PL decay curves of Tb^{3+}-doped $Lu_2W_3O_{12}$ and $Lu_2Mo_3O_{12}$ phosphors prepared at 1000 °C.

4. Conclusions

In conclusion, by using a solid-state reaction method, the Tb^{3+}-doped and undoped $Lu_2W_3O_{12}$ and $Lu_2Mo_3O_{12}$ materials were prepared under different calcine temperatures. The XRD results suggest that the 5 mol% Tb^{3+}-doping did not cause apparent variations on the XRD patterns besides the diffraction intensities. The FE-SEM pictures and the particle size distribution statistics illustrate that the materials were all composed of micrometer particles and the $Lu_2W_3O_{12}$ samples had smaller particles than that of the $Lu_2Mo_3O_{12}$ samples. The EDS patterns confirmed the compositions of Lu, Mo or W, O, and/or Tb in the materials. The preparing of temperature-dependent PL excitation spectra suggested that the optimum preparation temperature was 1200 °C for Tb^{3+}-doped $Lu_2W_3O_{12}$ phosphors and 1100 °C for Tb^{3+}-doped $Lu_2Mo_3O_{12}$ phosphors, respectively. The Tb^{3+}-doped $Lu_2Mo_3O_{12}$ phosphors prepared at 1000 °C and 1100 °C presented equivalent CTB excitation intensities, and 1000 °C was selected as the calcine temperature to prepare and compare the Tb^{3+}-doped and undoped $Lu_2Mo_3O_{12}$ and $Lu_2W_3O_{12}$ materials. The Tb^{3+}-doped $Lu_2W_3O_{12}$ green phosphor showed a stronger PL excitation intensity of CTB than that of the Tb^{3+}-

doped $Lu_2Mo_3O_{12}$ green phosphor. For undoped and doped $Lu_2W_3O_{12}$ and $Lu_2Mo_3O_{12}$ materials, the values of E_g calculated from the DRS were 4.02, 4.06, 3.94, and 3.95 eV, respectively. The values of E_g of the $Lu_2W_3O_{12}$ materials were larger than that of the $Lu_2Mo_3O_{12}$ materials. The measuring temperature dependent spectra indicated that the values of activation energy E_a of the Tb^{3+}-doped $Lu_2Mo_3O_{12}$ phosphors were 0.202 eV and 0.401 eV with 260 nm and 380 nm excitation, respectively, whereas the Tb^{3+}-doped $Lu_2W_3O_{12}$ phosphor illustrated a thermal enhancing CTB excitation intensity at 170 °C. The PL decay curves suggested that the lifetime corresponding to the $^5D_4$ level of Tb^{3+} was longer in the $Lu_2W_3O_{12}$ host lattice than in the $Lu_2Mo_3O_{12}$ host lattice. The Tb^{3+}-doped $Lu_2W_3O_{12}$ showed potential as an application in temperature sensors.

Author Contributions: Conceptualization, C.C. and A.X.; methodology, N.H., M.Z. and Z.C.; formal analysis, B.B., N.H., M.Z., Z.C. and C.C.; investigation, B.B., N.H., M.Z., Z.C. and C.C.; data curation, Y.L., B.B. and N.H.; writing—original draft preparation, N.H., G.L. and B.B.; writing—review and editing, G.L., Y.L. and C.C.; supervision, C.C., Y.L. and A.X.; project administration, C.C. and A.X.; funding acquisition, C.C. and A.X. All authors have read and agreed to the published version of the manuscript.

Funding: The research work was supported by the Natural Science Foundation of Fujian Province (Grant no. 2021J011207), the Open Fund of Fujian Provincial Key Laboratory of Functional Materials and Applications (Xiamen University of Technology fma2022006), the Key Project of Natural Science Foundation of Fujian Province (Grant no. 2020J02049), the Key Technical Innovation and Industrialization Projects of Fujian Province (Grant no. 2022G049), and the Major Project of Science and Technology of Xiamen City (Grant nos. 3502ZCQ20201001).

Institutional Review Board Statement: Not applicable.

Informed Consent Statement: Not applicable.

Data Availability Statement: Not applicable.

Conflicts of Interest: The authors declare no conflict of interest.

References

1. Shi, S.K.; Li, K.Y.; Wang, S.P.; Zong, R.L.; Zhang, G.L. Structural characterization and enhanced luminescence of Eu-doped $2CeO_2$–$0.5La_2O_3$ composite phosphor powders by a facile solution combustion synthesis. *J. Mater. Chem. C* **2017**, *5*, 4302–4309. [CrossRef]
2. Lu, J.F.; Mu, Z.F.; Zhu, D.Y.; Wang, Q.; Wu, F.G. Luminescence properties of Eu^{3+} doped $La_3Ga_5GeO_{14}$ and effect of Bi^{3+} co-doping. *J. Lumin.* **2018**, *196*, 50–56. [CrossRef]
3. Li, W.F.; Qiu, M.F.; Li, Y.X.; Zhang, S.A.; Li, Q.F.; Lin, W.X.; Mu, Z.F.; Wu, F.G. Energy Transfer and Multicolor-Tunable Emissions of $Sr_3La_6(SiO_4)_6$: Ce^{3+}, Tb^{3+}, Eu^{3+}. *J. Electron. Mater.* **2020**, *49*, 1404–1411. [CrossRef]
4. Mu, Z.F.; Hu, Y.H.; Chen, L.; Wang, X.J.; Ju, G.F.; Yang, Z.F.; Jin, Y.H. A single-phase, color-tunable, broadband-excited white light-emitting phosphor Y_2WO_6: Sm^{3+}. *J. Lumin.* **2014**, *146*, 33–36. [CrossRef]
5. Nair, G.B.; Swart, H.C.; Dhoble, S.J. A review on the advancements in phosphor-converted light emitting diodes (pc-LEDs): Phosphor synthesis, device fabrication and characterization. *Prog. Mater. Sci.* **2020**, *109*, 100622. [CrossRef]
6. Liu, X.; Li, L.; Noh, H.M.; Moon, B.K.; Choi, B.C.; Jeong, J.H. Chemical bond properties and charge transfer bands of O^{2-}-Eu^{3+}, O^{2-}-Mo^{6+} and O^{2-}-W^{6+} in Eu^{3+}-doped garnet hosts $Ln_3M_5O_{12}$ and ABO_4 molybdate and tungstate phosphors. *Dalton Trans.* **2014**, *43*, 8814–8825. [CrossRef]
7. Li, H.Y.; Yang, H.K.; Moon, B.K.; Choi, B.C.; Jeon, J.H.; Jang, K.W.; Lee, H.S.; Yi, S.S. Crystal Structure, Electronic Structure, and Optical and Photoluminescence Properties of Eu(III) Ion-Doped $Lu_6Mo(W)O_{12}$. *Inorg. Chem.* **2011**, *50*, 12522–12530. [CrossRef]
8. Lee, G.H.; Kim, T.H.; Yoon, C.; Kang, S. Effect of local environment and Sm^{3+}-codoping on the luminescence properties in the Eu^{3+}-doped potassium tungstate phosphor for white LEDS. *J. Lumin.* **2008**, *128*, 1922–1926. [CrossRef]
9. Baur, F.; Jüstel, T. (INVITED) Eu^{3+} activated molybdates—Structure property relations. *Opt. Mater. X* **2019**, *1*, 100015. [CrossRef]
10. Cao, C.Y.; Zhang, Z.J.; Wei, S.J.; Xie, A.; Noh, H.M.; Jeong, J.H. Synthesis, optical properties, energy transfer, thermal behavior, and LED package of Eu^{3+} doped lutetium tungsten oxide phosphors. *Opt. Mater.* **2020**, *101*, 109753. [CrossRef]
11. Cao, C.Y.; Wei, S.J.; Zhu, Y.X.; Liu, T.; Xie, A.; Noh, H.M.; Jeong, J.H. Synthesis, optical properties, and packaging of Dy^{3+} doped Y_2WO_6, $Y_2W_3O_{12}$, and Y_6WO_{12} phosphors. *Mater. Res. Bull.* **2020**, *126*, 110846. [CrossRef]
12. Yan, S.; Zhang, J.; Zhang, X.; Lu, S.; Ren, X.; Nie, Z.; Wang, X. Enhanced red emission in $CaMoO_4$:Bi^{3+}, Eu^{3+}. *J. Phys. Chem. C* **2007**, *111*, 13256–13260. [CrossRef]

13. Zhou, Y.; Yan, B. $RE_2(MO_4)_3$: Ln^{3+}(RE = Y, La, Gd, Lu; M = W, Mo; Ln = Eu, Sm, Dy) microcrystals: Controlled synthesis, microstructure and tunable luminescence. *CrystEngComm* **2013**, *15*, 5694–5702. [CrossRef]
14. Li, L.; Shen, J.; Zhou, X.J.; Pan, Y.; Chang, W.X.; He, Q.W.; Wei, X.T. Luminescent properties of Lu_2MoO_6:Eu^{3+} red phosphor for solid state lighting. *Trans. Nonferr. Met. Soc. China* **2016**, *26*, 1670–1675. [CrossRef]
15. Guan, L.; Wei, W.; Guo, S.Q.; Su, H.X.; Li, X.; Shang, Y.X.; Yang, Z.P.; Guo, Q.L.; Fu, G.S. Fabrication and Luminescent Properties of Tb^{3+} Doped Double Molybdate Phosphors. *J. Electrochem. Soc.* **2012**, *159*, D200–D203. [CrossRef]
16. Mahlik, S.; Diaz, F.; Boutinaud, P. Luminescence quenching in $KYb(WO_4)_2$-Tb^{3+}: An example of temperature-pressure equivalence. *J. Lumin.* **2017**, *191*, 18–21. [CrossRef]
17. Chen, X.Y.; Zhang, Z.J.; Feng, A.; Xu, M.; Zhao, J.T.; Xu, F.F. Electronic structure, optical and thermal/concentration quenching properties of $Lu_{2-2x}Eu_{2x}WO_6$ ($0 \leq x \leq 0.2$). *Mater. Res. Bull.* **2015**, *70*, 26–31. [CrossRef]
18. Dang, P.P.; Li, G.G.; Yun, X.H.; Zhang, Q.Q.; Liu, D.J.; Lian, H.Z.; Shang, M.M.; Lin, J. Thermally stable and highly efficient red-emitting Eu^{3+}-doped $Cs_3GdGe_3O_9$ phosphors for WLEDs: Non-concentration quenching and negative thermal expansion. *Light Sci. Appl.* **2021**, *10*, 29. [CrossRef] [PubMed]
19. Geng, X.; Xie, Y.; Chen, S.S.; Luo, J.M.; Li, S.C.; Wang, T.; Zhao, S.C.; Wang, H.; Deng, B.; Yu, R.J.; et al. Enhanced local symmetry achieved zero-thermal-quenching luminescence characteristic in the Ca_2InSbO_6:Sm^{3+} phosphors for w-LEDs. *Chem. Eng. J.* **2021**, *410*, 128396. [CrossRef]
20. Zou, H.; Yang, X.Q.; Chen, B.; Du, Y.Y.; Ren, B.Y.; Sun, X.Q.; Qiao, X.S.; Zhang, Q.W.; Wang, F. Thermal Enhancement of Upconversion by Negative Lattice Expansion in Orthorhombic $Yb_2W_3O_{12}$. *Angew. Chem. Int. Ed.* **2019**, *58*, 17255–17259. [CrossRef]
21. Zou, H.; Chen, B.; Hu, Y.F.; Zhang, Q.W.; Wang, X.S.; Wang, F. Simultaneous Enhancement and Modulation of Upconversion by Thermal Stimulation in $Sc_2Mo_3O_{12}$ Crystals. *J. Phys. Chem. Lett.* **2020**, *11*, 3020–3024. [CrossRef] [PubMed]
22. Cao, C.Y.; Xie, A.L.; Zhou, T.L.; Zhong, H.C.; Lu, X.J.; Xie, A.; Noh, H.M.; Jeong, J.H. Eu^{3+} doped lutetium molybdenum oxides: Synthesis, optical properties, thermal behavior, and LED packaging. *J. Lumin.* **2020**, *217*, 116759. [CrossRef]
23. Chen, Z.J.; Cao, C.Y.; Zhang, M.; Huang, N.H.; Bai, B.H.; Yang, L.; Li, Y.C.; Xie, A. Thermal enhancing photoluminescence intensities of Eu^{3+} doped $Lu_2(MoO_4)_3$. *Opt. Mater.* **2022**, *127*, 112301. [CrossRef]
24. Sumithra, S.; Umarji, A.M. Negative thermal expansion in rare earth molybdates. *Solid State Sci.* **2006**, *8*, 1453–1458. [CrossRef]
25. Nugent, L.J.; Baybarz, R.D.; Burnett, J.L.; Ryan, J.L. Electron-transfer and f-d absorption bands of some lanthanide and actinide complexes and the standard (II–III) oxidation potential for each member of the lanthanide and actinide series. *J. Phys. Chem. C* **1973**, *77*, 1528–1539. [CrossRef]
26. Baur, F.; Glocker, F.; Jüstel, T. Photoluminescence and energy transfer rates and efficiencies in Eu^{3+} activated $Tb_2Mo_3O_{12}$. *J. Mater. Chem. C* **2015**, *3*, 2054–2064. [CrossRef]
27. Liu, Y.X.; Yue, X.J.; Cai, K.; Deng, H.D.; Zhang, M. Microwave-assist hydrothermal synthesis and luminescence of $NaGd(WO_4)$:Tb^{3+} phosphors: A case study for the energy saving in the synthesis of phosphors. *Energy* **2015**, *93*, 1413–1417. [CrossRef]
28. Zeng, W.; Wang, Y.H.; Han, S.C.; Chen, W.B.; Li, G.; Wang, Y.Z.; Wen, Y. Design, synthesis and characterization of a novel yellow long-persistent phosphor: Ca_2BO_3Cl:Eu^{2+}, Dy^{3+}. *J. Mater. Chem. C* **2013**, *17*, 3004–3011. [CrossRef]
29. Cao, G.; Rabenberg, L.; Nunn, C.M.; Mallouk, T.E. Formation of quantum-size semiconductor particles in a layered metal phosphonate host lattice. *Chem. Mater.* **1991**, *3*, 149–156. [CrossRef]
30. Materials Project. Available online: https://materialsproject.org/materials/mp-768455?chemsys=Lu-W-O (accessed on 10 November 2021).
31. Wang, B.; Li, X.S.; Zeng, Q.G.; Yang, G.T.; Luo, J.Y.; He, X.; Chen, Y.Q. Efficiently enhanced photoluminescence in Eu^{3+}-doped $Lu_2(MoO_4)_3$ by Gd^{3+} substituting. *Mater. Res. Bull.* **2018**, *100*, 97–101. [CrossRef]
32. Zhang, M.; Cao, C.Y.; Zhang, C.L.; Chen, Z.J.; Bai, B.H.; Huang, N.H.; Xie, A. Synthesis and Luminescent Properties of $Gd_{2[1-x(y)]}Eu_{2x(y)}W_zMo_{(1-z)}O_6$ Red Phosphors. *Chin. J. Lumin.* **2022**, *43*, 1086–1094. [CrossRef]
33. Ueda, J.; Dorenbos, P.; Bos, A.J.J.; Meijerink, A.; Tanabe, S. Insight into the Thermal Quenching Mechanism for $Y_3Al_5O_{12}$:Ce^{3+} through Thermoluminescence Excitation Spectroscopy. *J. Phys. Chem. C* **2015**, *119*, 25003–25008. [CrossRef]
34. Kim, Y.H.; Arunkumar, P.; Kim, B.Y.; Unithrattil, S.; Kim, E.; Moon, S.H.; Hyun, J.Y.; Kim, K.H.; Lee, D.; Lee, J.S.; et al. A Zero-thermal-quenching Phosphor. *Nat. Mater.* **2017**, *16*, 543–550. [CrossRef] [PubMed]
35. Xu, S.C.; Wang, Z.J.; Li, P.L.; Li, T.; Bai, Q.Y.; Sun, J.; Yang, Z.P. Single-phase white-emitting phosphors $Ba_3Ce_{(1-x-y)}(PO_4)_3$:xTb^{3+}, yMn^{2+} and $Ba_3Ce_{(1-x-z)}(PO_4)_3$:xTb^{3+},zSm^{3+}: Structure, luminescence, energy transfer and thermal stability. *RSC Adv.* **2017**, *7*, 19584–19592. [CrossRef]
36. Tian, M.M.; Li, P.L.; Wang, Z.J.; Teng, X.Y.; Li, Z.L.; Cheng, J.G.; Sun, Y.S.; Wang, C.; Yang, Z.P. Synthesis, color-tunable emission, thermal stability, luminescence and energy transfer of Sm^{3+} and Eu^{3+} single-doped $M_3Tb(BO_3)_3$ (M = Sr and Ba) phosphors. *CrystEngComm* **2016**, *18*, 6934–6947. [CrossRef]
37. Wang, Y.; Deng, B.; Ke, Y.; Shu, S.; Liu, R.X.; Yu, R.J. Spectroscopic investigation of $La_7Ta_3W_4O_{30}$:Sm^{3+} orange-red phosphor for white LEDs. *Arab. J. Chem.* **2020**, *13*, 5581–5592. [CrossRef]
38. Bhushan, S.; Chukichev, M.V. Temperature dependent studies of cathodoluminescence of green band of ZnO crystals. *J. Mater. Sci. Lett.* **1988**, *7*, 319–321. [CrossRef]
39. Qiao, J.; Zhang, Z.C.; Zhao, J.; Xia, Z.G. Tuning of the Compositions and Multiple Activator Sites toward Single-Phased White Emission in $(Ca_{9-x}Sr_x)MgK(PO_4)_7$:$Eu^{2+}$ Phosphors for Solid-State Lighting. *Inorg. Chem.* **2019**, *58*, 5006–5012. [CrossRef]